JMEPEG (1998) 7:479-490

Study of Dynamic Explicit Analysis in Sheet Metal Forming Processes Using Faster Punch Velocity and Mass Scaling Scheme

D.W. Jung

(Submitted 21 August 1997; in revised form 8 April 1998)

A finite element formulation using dynamic explicit time integration scheme is developed for numerical analysis of autobody panel stamping processes. The lumping scheme is employed for the diagonal mass matrix and linearizing dynamic formulation. A contact scheme is developed by combining the skew boundary condition and direct trial and error method. To investigate the effects of punch velocity, various values of punch velocity are used for numerical analysis. The mass scaling scheme is introduced for economic analysis. To investigate the effects of mass scaling, various mass scalings are used. Computations are performed for analysis of complicated autobody panel stamping processes including the formation of an oilpan and a fuel tank.

Keywords autobody panel stamping, dynamic explicit, finite element method, mass scaling, punch velocity, sheet metal forming

1. Introduction

Sheet metal forming is currently one of the principal manufacturing processes in the automotive industry, aerospace industry, electrical device industry, kitchenware industry, and so on. The successful applications of sheet metal forming and the popularity of sheet metal products are attributable to their relatively light weight, low cost due to mass production, good surface finish, near net shaping of final products, and great interchangeability. From the viewpoint of mechanics, the deformation problems of sheet metal working are nonlinear problems in geometry, material behavior, and contact phenomena. The knowledge of the deformation mechanics and the influence of the process variables are important in the design of sheet metal working processes. Such information allows better design criteria for actual forming processes. The trial and error procedures based on the experiences used for designing the processes are expensive, and these often result in long lead times in developing new sheet metal parts. To reduce the tooling lead time and cost in die development, an integrated approach of computer-aided design/computer-aided manufacturing/computer-aided engineering system, which modifies the design on the basis of formability analysis, has been introduced in many automotive companies. Process modelling by a systematic method of simulation such as the finite element method may be used as a tool to improve the quality of the product and to reduce the dependence on skilled tool and die makers.

The finite element method has long been used as a means of reliable computation to analyze various sheet metal forming processes. Starting from two-dimensional analyses of sheet forming processes, various analyses have been performed by the implicit method based on the direct matrix solver, as well as by the explicit method based on dynamic solutions (Ref 1-7).

For simple two-dimensional analyses, the implicit method of analysis seems to appear significantly more efficient, because it provides better solution accuracy than the explicit method. The explicit method required relatively large amounts of computer time due to the stringent limitation in time increment imposed by the stability condition. As a consequence, much of the efforts for development in the following years has been concentrated on the implicit methods. The successful use of two-dimensional finite element analyses has led to a natural extension of the implicit methods to three-dimensional problems appearing rather straightforward (Ref 8-10). However, the transition to three-dimensional forming problems brought about many unexpected difficulties. In particular, the variable contact conditions caused a number of problems, including the problem of stable convergency. This led to a renewed interest in the application of the explicit method based on dynamics to essentially quasi-static sheet forming problems. In the explicit method, the size of time increment must be determined by the limitation in stability, but must not be significantly affected by the increased number of contact points.

The explicit dynamic algorithm has several significant advantages over the conventional implicit static algorithm for sheet metal forming problems (Ref 11, 12). In the explicit method, there is no banded equation solver like the Newton-Raphson method. Consequently, the computational cost of a solution does not grow quadratically with the problem size. In general, the computational cost is linearly proportional with the problem size in the explicit dynamic procedure. Recently, the dynamic explicit type of the finite element method has been used more often in industry, especially by the commercial codes. The major disadvantage of the explicit dynamic procedure is due to the fact that it is a time and rate dependent dynamic procedure that sometimes loses static stability of a solution. Generally, this requires that some sort of artificial time scale must be introduced into the analysis to achieve an

D.W. Jung, Department of Mechanical Engineering, Cheju National University, Cheju-Do, Cheju city, 690-756, South Korea. Contact e-mail: jdwcheju@cheju.cheju.ac.kr.

economical solution. Dynamic sheet metal forming analysis is performed at the fast punch velocities around the order of 5 to 20 m/s, with the assumption that this approximates the quasi-static solutions. In the same way, for economic analysis, the mass scaling scheme is used, with approximately 10 to 60 times the real density, which does not affect solution reliability. A finite element program using dynamic explicit time integration scheme is developed for numerical analysis of autobody panel stamping processes (Ref 7, 11), and a study of the effects on the results of dynamic explicit analysis by using the faster punch velocity and the mass scaling scheme is performed.

2. Theory

2.1 General Description of the Dynamic Explicit Formulation

A nonlinear finite element equation of motion is obtained from the principle of virtual work, which is the weak form for equilibrium equation. The weak form, which includes internal force, contact/friction force, inertia force, damping force, external force, and boundary condition, is described as follows (Ref 11):

$$\int_{V_0} S\delta E dv + \int_{V_0} \rho_0 \ddot{x}\delta u dv - \int_{V_0} \rho_0 b\delta u dv - \int_s F_0 \delta u ds + \sum_{i=1}^{1} \int_{S_i} \frac{(P^i_c \delta g^i_n + \tau_c \delta g^i_T)}{\text{contact + friction}} dS = 0 \quad \text{(Eq 1)}$$

where S means the surface, which is subjected to the external force, and S_i means the surface in contact. The left side of the above equation includes the terms for internal work, inertia work, work done by body force, work exerted by the stress boundary condition, and work consumption due to contact and friction. In finite element discretization of the above equation, the internal work term includes either material behavior model or kinematic model according to element types.

If membrane model, material behavior model, element shape function, and dynamics of rigid body are introduced into the principle of virtual work, a nonlinear finite element equation of motion can be obtained. The nonlinear finite element equation can be expressed by the following matrix form at time step n.

$$[M]\{\ddot{u}_n\} + [C]\{\dot{u}_n\} + \{P_n\} - \{F_n\} + \{R_{cn}\} = 0 \quad \text{(Eq 2)}$$

From the above equation, to obtain a solution at time step $n + 1$, the central difference method for the time discretization of acceleration and velocity is introduced:

$$\ddot{u}_n = \frac{\dot{u}_{n+1/2} - \dot{u}_{n-1/2}}{\Delta t} = \frac{u_{n+1} - 2u_n + u_{n-1}}{2\Delta t^2}$$

$$\dot{u}_{n+1/2} = \frac{u_{n+1} - u_n}{\Delta t} \text{ or } \dot{u}_n = \frac{u_{n+1} - u_{n-1}}{2\Delta t} \quad \text{(Eq 3)}$$

If the above equation is substituted into Eq 2 and rearranged, the following equation can be obtained:

$$\left(\frac{M}{\Delta t^2} + \frac{C}{2\Delta t}\right) u_{n+1} = F_n - P_n - R_{cn} + \frac{M}{\Delta t^2} u_n - \left(\frac{M}{\Delta t^2} - \frac{C}{2\Delta t}\right) u_{n-1} \quad \text{(Eq 4)}$$

The central difference method has selective convergency according to the magnitude of Δt, and the accuracy and convergency are linearly proportional to the square of Δt (Ref 13). Nodal displacements can be obtained at time step $n + 1$ by Eq 4; then the deformation area is updated. A new magnitude of time increment to guarantee convergency should be decided according to the updated deformation. The magnitude of global time increment can be determined by the following equation after calculating the time increment of every element.

$$\Delta t_{n+1} = \alpha \min\{\Delta t_1, \Delta t_2, \ldots, \Delta t_N\} \quad \text{(Eq 5)}$$

where N is the total element number and Δt_i is the time increment of the ith element. The safe constant, α, is often selected to be less than 0.9.

The critical time increment is determined:

$$\Delta t_c = L_s / C \quad \text{(Eq 6)}$$

where L_s is the characteristic length, which is the given element area divided by the largest edge.

The propagation speed C is determined:

$$C = \sqrt{\frac{E_t}{\rho}} \quad \text{(Eq 7)}$$

where E_t is the tangent modulus and ρ is material density.

A mass scaling scheme is introduced because the time scale of the analysis is of particular importance in dynamic analysis. In this case, the analysis cannot simply be sped up without affecting the results because the inertial effects are not the only criteria to consider. One approach is to scale the mass density while using the real process time:

- The wave speed of the material is inversely proportional to the square root of the material density.
- Increasing the density by a factor of 100 will increase the stable time increment by a factor of 10.
- The effect is to increase the ratio of material wave speed to the punch speed.

Mass scaling allows for the use of unaltered material properties with the same process time.

The explicit procedure is a true dynamic procedure and was originally developed for high speed impact problems. Because of the robust nature of the contact algorithms and the ability to model extremely large problems, investigators often try to analyze low speed events with the dynamic explicit procedure. Even quasi-static problems can be attempted using the explicit scheme. In realistic metal forming or stamping processes, a

punch may move at speeds of 1 m/s or less, and the forming process may occur over a time period of seconds. These rates are very slow compared to typical wave speeds in metals. The wave speed in steel is approximately 5000 m/s. The problem should be run at the highest punch speed at which the inertial effects do not dominate the solution. In general, the punch velocity must be less than one percent of the wave speed of the material to obtain a reasonable static solution.

2.2 Lumping Scheme

The computational efficiency and accuracy of the explicit procedure is based on the implementation of an explicit integration rule along with the use of lumped element mass matrices.

$$[M]\,[a] = [F]$$
$$[a] = [M]^{-1}[F] \qquad \text{(Eq 8)}$$

If matrix [*M*] is lumped as a diagonal matrix, matrix inversion is not needed, and a solution can be obtained directly by a linear equation, $a_i = m_i^{-1} f_i$. The lumping scheme is computationally economic because matrix inversion involves large computing time. Often in dynamic analysis, the use of lumping mass renders more accurate results than consistent mass (Ref 13-16).

The lumping scheme is expressed:

$$m^{e}_{pq} = \begin{cases} \alpha\delta_{ij}\int_{\Omega^e} \rho N_a^2\, d\Omega & a = b \\ 0 & a \neq b \end{cases} \qquad \text{(Eq 9)}$$

where

$$\alpha = \frac{\int_{\Omega^e} \rho d\Omega}{\text{total element}} \Big/ \frac{\left(\sum_{a=1}^{n_{eg}} \int_{\Omega^e} \rho N_a^2 d\Omega\right)}{\text{amount of diagonal entries of consistent mass}}$$

where Ω^e is element domain, *p* and *q* are element equation numbers, and *a* and *b* are element node numbers. In this method, lumped mass is proportional to the diagonal part of the consistent mass matrix, and the positive valued lumped mass can always be obtained. In the above equation, the constant α is used to conserve the total element mass.

2.3 The Efficient Contact and Friction Treatment Scheme for Dynamic Explicit Integration

The explicit contact algorithm takes advantage of a small time increment required by the stability limit (Ref 11, 12, 14). The use of small increments is advantageous because it drastically simplifies the implementation of contact conditions.

The contact and friction scheme is the mixed form of the skew boundary condition and the direct trial and error method (Ref 11, 13). The accelerations, velocities, and displacements are first calculated without taking the contact conditions into consideration. Then, the penetration distance *h*, the tool normal direction, and the sheet normal direction of contact points are calculated as shown in Fig. 1.

From the above calculation, the skew boundary condition is applied, and the resisting force to prevent the penetration of a node is readily calculated as:

$$N = mh\mathbf{n}/\Delta t^2 \qquad \text{(Eq 10)}$$

where *m* is a nodal lumping mass, and **n** is a normal vector. If it is assumed that the motion of the tools is not influenced by the contact itself, the acceleration changes:

$$a = a_{pred} + a_{corr} = a_{pred} + N/m \qquad \text{(Eq 11)}$$

and the corrections to the velocity and displacement are calculated:

$$V = V_{pred} + a_{corr}\Delta t$$
$$u = u_{pred} + V_{corr}\Delta t \qquad \text{(Eq 12)}$$

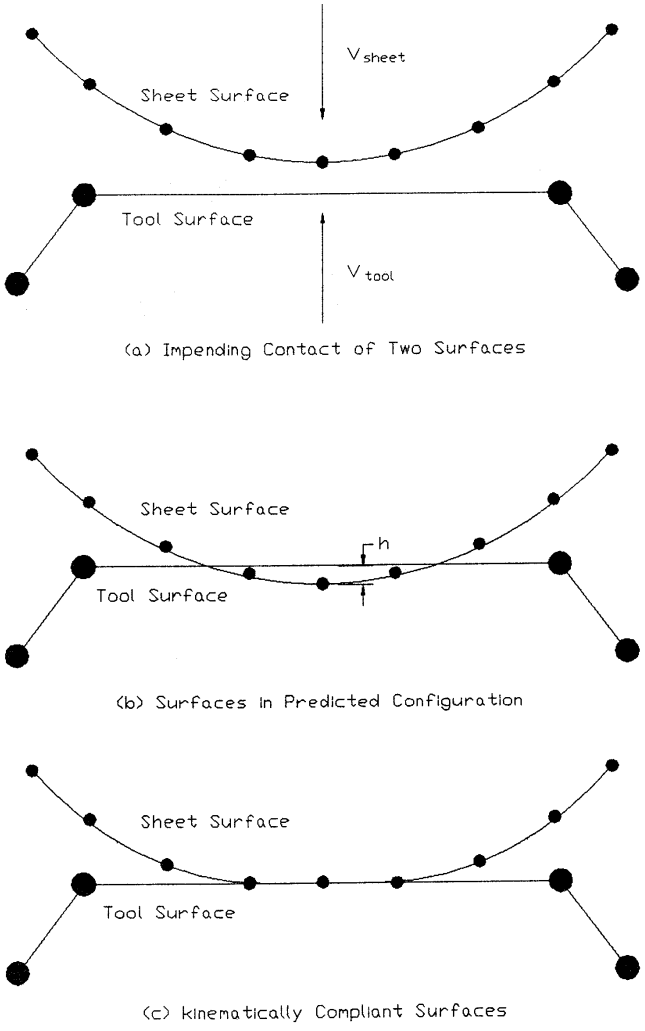

Fig. 1 Schematic description for the contact scheme

For friction, the increment is first solved without taking friction into consideration, and the skew boundary condition is applied as shown in Fig. 2. Under the skew boundary condition, it is not necessary to define surface directions t_c along which a slip increment r_c is measured. The resisting force T_c required to prevent slip is then calculated in the same way as the calculation of the force required to prevent penetration:

$$T_c = -mr_c/\Delta t^2 \quad \text{(Eq 13)}$$

where r_c is the slip increment.

Accordingly, the friction force is calculated as follows:

$$T_{frict} = \frac{T_c}{|T_c|} \min (T_{cr}, |T_c|) \quad \text{(Eq 14)}$$

The resisting force $|T_c|$ is compared with the critical force $T_{cr} = \mu|N|$. If the resisting force is less than the critical force, a sticking condition is assumed, and then the resisting force is simply applied. If the resisting force is larger than the critical force, a slipping condition is assumed, and the friction force is assumed to obey Coulomb's friction law. The procedures of friction force calculation and stick/slip check are summarized in Fig. 3.

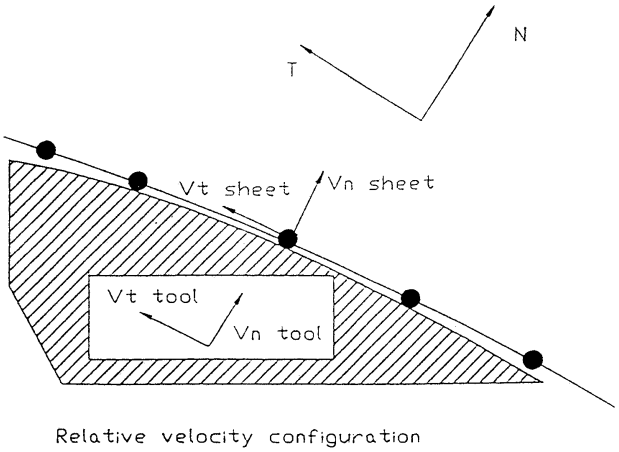

Fig. 2 Schematic description for friction and stick/slip check

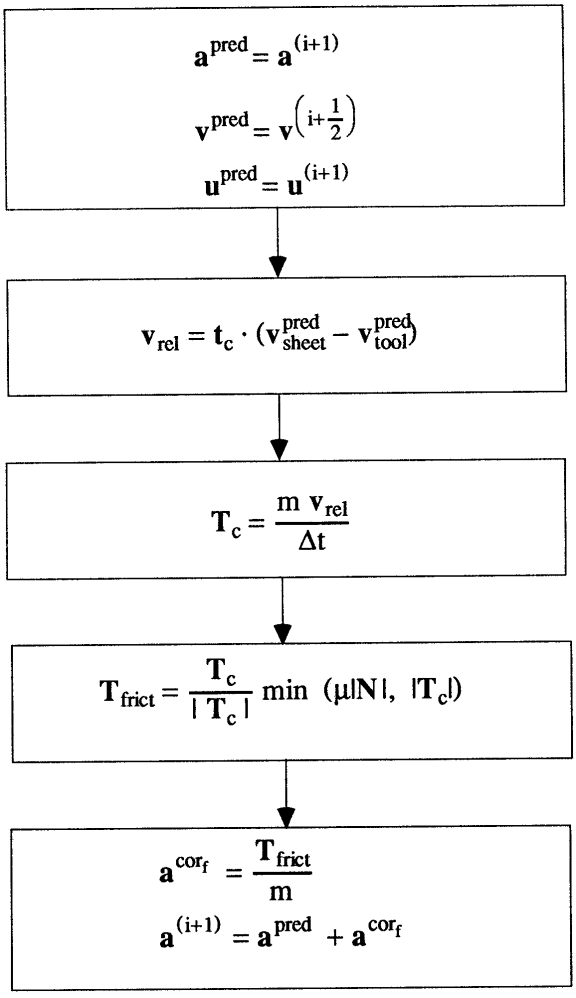

Fig. 3 Flow chart for friction force calculation and stick/slip check

3. Results and Discussion

3.1 Deep Drawing of an Oilpan

Deep drawing of an oilpan involves a complicated three-dimensional deformation during the sheet forming process. Due to complex geometry, sliding and contact of sheet material occurs from region to region. Because the drawing depth is quite large compared with the original size of the sheet blank, the oilpan as a part of automobile engine is difficult to form, and the flatness of the flange is important. Until recently, finite element simulation for deep drawing of a rectangular box shaped and stepped part was mainly performed by using the

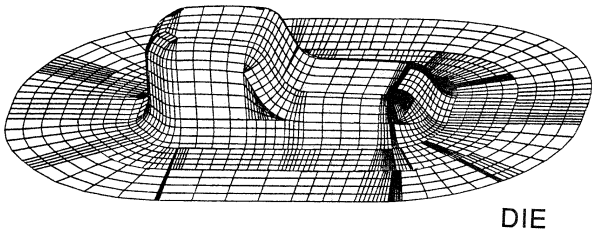

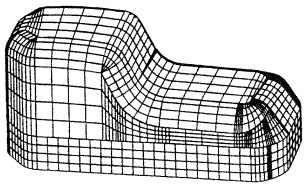

	surfaces	patches
punch	*55*	*97*
die	*80*	*174*
Σ	*135*	*271*

Fig. 4 Schematic view of the parametric tool surfaces for oilpan deep drawing

explicit commercial packages based on elastic plastic shell elements. Vreede et al. (Ref 17) analyzed the forming processes for the headlight bracket of a truck, and Liu and Karima (Ref 18) predicted the initial blank shape of an oilpan by using one step finite element approach based on the upper-bound theorem from the viewpoint of design concept. The rigid tool was modeled by CATIA (Computer Aided Three Dimensional Interactive Application) CAD/CAM system (Dassault Co., Cedex, France). Figure 4 shows the schematic view of the tool parametric surfaces in which 135 composite surfaces (271 patches) are used to describe the punch and the die.

Figure 5 shows the finite element mesh used for the analysis with 1251 nodes and 2400 triangular elements. The blank has an original rectangular shape of 560 mm by 440 mm. The material and process variables used in the analysis are as follows:

- Initial sheet thickness, 1.2 mm
- Stress-strain curve, $\overline{\sigma} = 451.8\ (\overline{\varepsilon} + 0.008)^{0.306}$ MPa
- Lankford value for normal anisotropy, $r = 1.984$
- Coulomb coefficient of friction, $\mu = 0.1$
- Blankholding force, 860 kN

Figure 6 shows the deformed experimental shape at the final punch stroke. The practical product contains embossed reinforcements to impose the rigidity in the middle part of the product and has the draw beads. In the simulation, however, the tool was simplified for obtaining simulation results by ignoring the embossing and draw beads because of the limitation of analysis code. The blankholding force used in analysis is larger than the realistic blankholding force used in the experiment (approximately 720 kN) because of (or instead of) ignoring the draw beads.

To investigate the effects of punch velocity, various values of punch velocity, that is, 15 m/s, 25 m/s, 35 m/s, and 70m/s are used with the mass scaling in which the density is increased by a factor of 50 for numerical analysis in Fig. 7 and 8. Figure 7 shows the predicted deformed configurations at selected punch velocity. As the punch velocity is increased, the inertia effect becomes larger, and force cannot be sufficiently transmitted to the nodes located at the outerside of the blank. Also, the deformed configurations of the flange show less drawing-in (Ref 19, 20). Accordingly, the thickness strain distribution at a chosen section is higher deviating from reasonable distribution as the punch velocity is increased as shown in Fig. 8. The numerical results for the punch velocity of 15 m/s are similar to the static implicit results of using the same material and process variables. This punch velocity has proven to be a good compromise between accuracy and effectiveness. In this example, the comparison with experimental results is unreasonable because of simulating with the tool of ignoring the embossing and draw beads. The results of dynamic explicit analysis are compared with the results of static implicit analysis. The static implicit code is already developed for the research pertaining to the autobody panel stamping processes. The whole computation time for the static implicit scheme took approximately 15 h with two restarts in Hp/730 workstation. For the dynamic explicit case of 15 m/s punch velocity, it took approximately 7 h. For the dynamic explicit case of 25 m/s punch velocity, it took approximately 4 h. For the case of 35 m/s, it took approximately 2.7 h. For the case of 70 m/s, it took approximately 1.34 h.

For economic analysis, the mass scaling method is introduced. To investigate the effects of mass scaling, the various

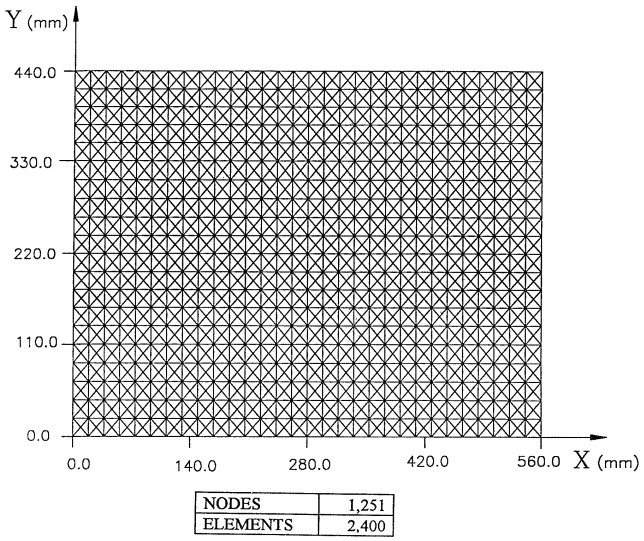

Fig. 5 Finite element mesh used in the analysis of deep drawing of an oilpan

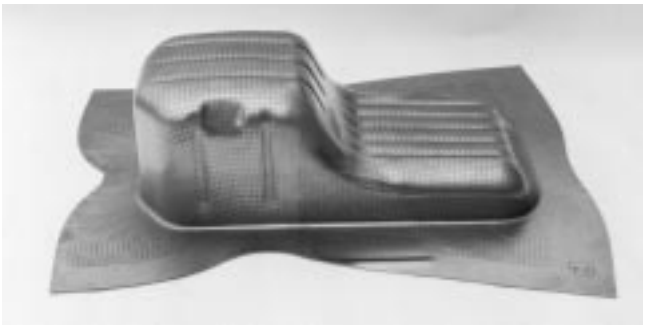

(a)

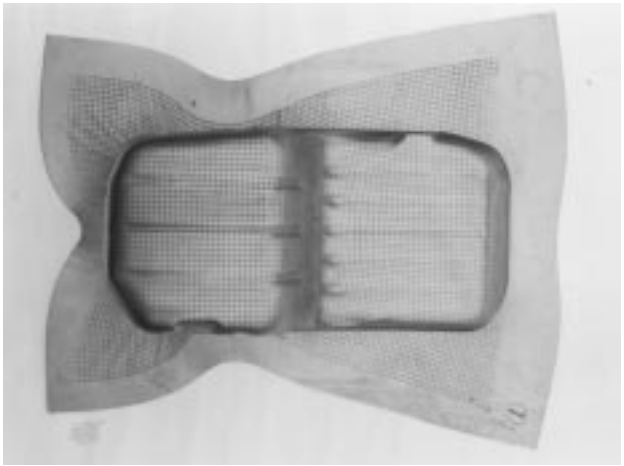

(b)

Fig. 6 Photographs of experimental specimens by oilpan deep drawing. (a) View-1. (b) View-2

mass scalings, which increase the density by factors of 50, 150, and 700 are used with 15 m/s punch velocity. Figure 9 shows the predicted deformed configurations, and Fig. 10 shows the thickness strain distribution at a chosen section. For punch velocity, the excessive increase in the mass scaling causes the deviation from reasonable solution. This phenomenon can be explained by the excessive increase of inertia energy due to large density. The mass scaling in which the density is increased by a factor of 50 is shown to provide a comparatively reasonable solution. The whole computation time for the dynamic explicit case of the mass scaling, in which the density is increased by a factor of 50, took approximately 7 h in Hp/730 workstation. For the dynamic explicit case of the mass scaling in which the density is increased by a factor of 150, it took approximately 3.67 h. For the dynamic explicit case of the mass scaling in which the density is increased by a factor of 700, it took approximately 1.67 h. The velocity scaling and mass scaling methods have identical effects on solution time and accuracy in attempting to find a static solution using a dynamic explicit formulation from simulation results because of not using the rate dependent material. If the rate dependent material is used, the effects of the two scaling methods may behave differently.

Figure 11 shows the thickness strain distribution and deformed configuration predicted by the simulation of the 15 m/s punch velocity and the 50 times mass scaling at the final stage. Figure 12 shows the comparison of the deformed edge contour predicted by the present analysis of the 15 m/s punch velocity

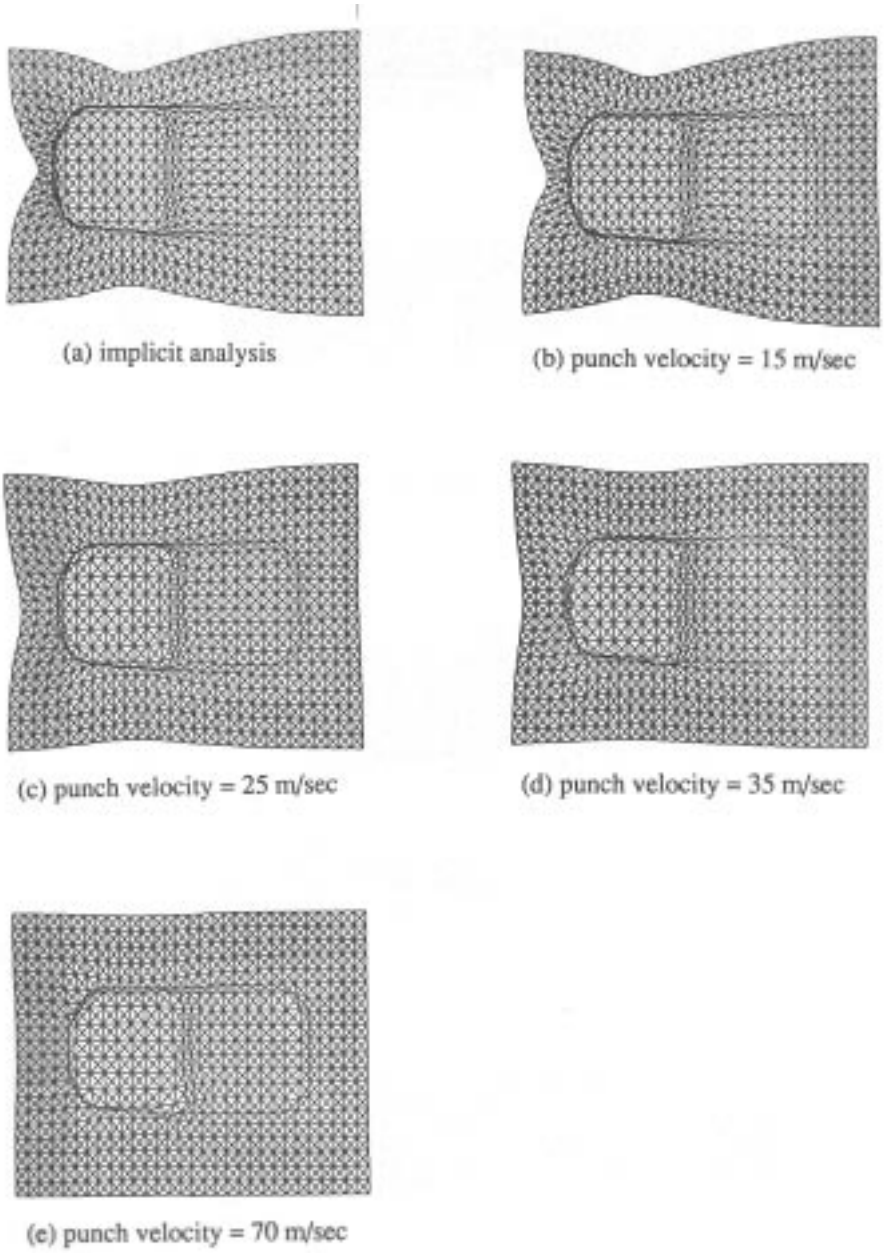

Fig. 7 Comparison of edge contour in oilpan deep drawing with various punch velocity

and the 50 times mass scaling with the experimental results. The edge contour is somewhat different from the experimental result. This discrepancy is partly due to the ignorance of embossings and draw beads. The deviation is able to be considered from the introduction of many assumptions for the efficient and simple analysis, the limitation of analysis code itself, and the measurement error of experimental results, and so on.

3.2 Deep Drawing of a Fuel Tank

A fuel tank is difficult to simulate because the tool surface has a stepped geometry to enhance the rigidity in the middle part of the product, and there exists higher-order nonlinearities of contact and friction. The rigid tool description is modelled by CATIA CAD/CAM system. Figure 13 shows the whole tool surface described with 31,800 nonparametric patches. The nonparametric patch has the advantage of a reduced computation time while the parametric patch is in connection with the contact search algorithm (Ref 21).

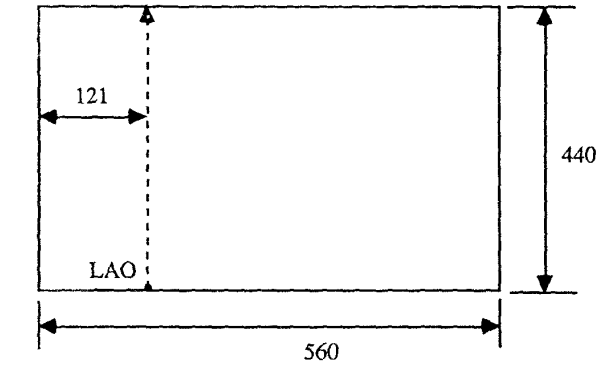

(a)

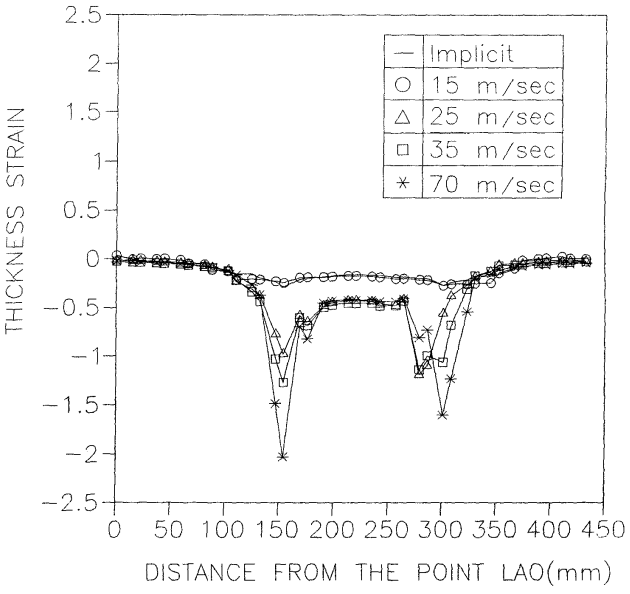

(b)

Fig. 8 Thickness strain distribution for the deep drawing of an oilpan with various punch velocity. (a) Base line on initial sheet blank for strain distribution measurement. (b) Comparison of thicknes strain distribution on the line

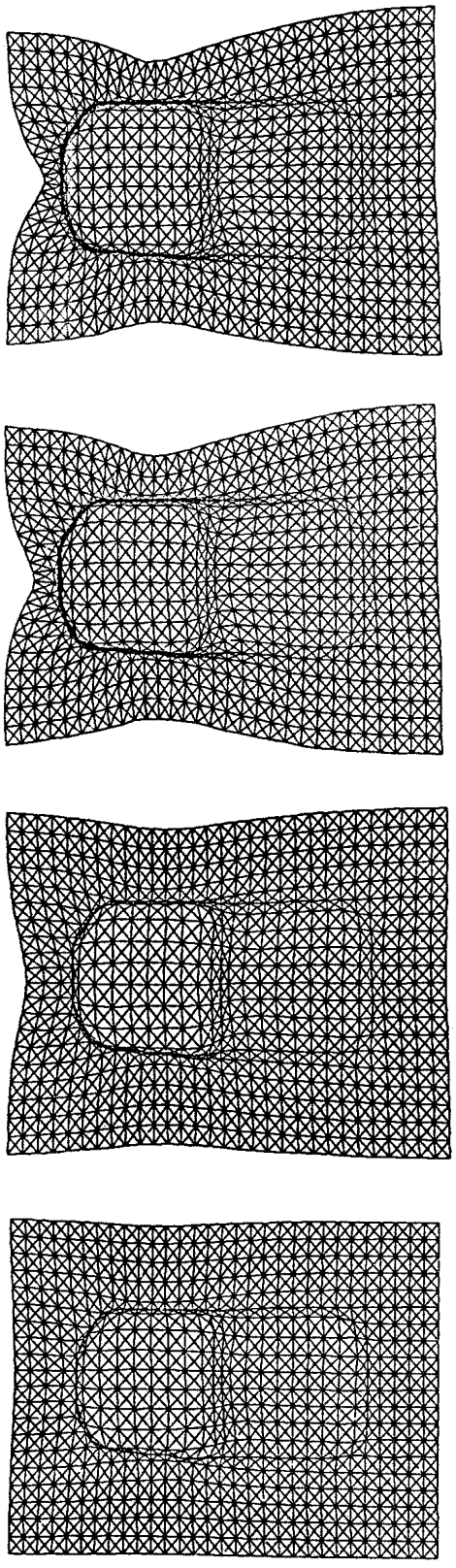

(a) **(b)** **(c)** **(d)**

Fig. 9 Comparison of edge contour in oilpan deep drawing with various mass scaling. (a) Implicit analysis. (b) Increasing the density by a factor of 50. (c) Increasing the density by a factor of 150. (d) Increasing the density by a factor of 700

The blank has an initial rectangular shape (1020 mm by 700 mm), and 2400 triangular elements are used.

The material and process variables used in the analysis are as follows:

- Initial sheet thickness, 0.8 mm
- Stress-strain curve, $\bar{\sigma} = 526.0(\bar{\varepsilon})^{0.239}$ MPa
- Lankford value for normal anisotropy, $r = 1.79$
- Coulomb coefficient of friction, $\mu = 0.1$
- Blankholding force, 900 kN

Figure 14 shows the deformed experimental shape at the final punch stroke. The practical product contains embossed reinforcements to impose the rigidity in the middle part of the product and has the draw beads. In the simulation, however, the tool was simplified for obtaining simulation results by ignoring the draw beads because of the limitation of analysis code. The blankholding force used in analysis is larger than the realistic blankholding force used in the experiment (approximately 750 kN) because of (or instead of) ignoring the draw beads.

To investigate the effects of punch velocity, various values of punch velocity, that is, 5 m/s, 10 m/s, 20 m/s, and 30 m/s are used with the mass scaling in which the density is increased by a factor of 50 for numerical analysis as shown in Fig. 15 and 16. Figure 15 shows the predicted deformed configurations at selected punch velocity. As the punch velocity is increased, the inertia effect becomes larger, and force cannot be sufficiently transmitted to the nodes located at the outerside of the blank. Also, the deformed configurations of the flange show less drawing-in. Accordingly, the thickness strain distribution at an arbitrarily chosen section is higher deviating from reasonable distribution as the punch velocity is increased as shown in Fig. 16. The numerical results for the punch velocity of 10 m/s are similar to the results for the punch velocity of 5 m/s. These results also agree with the experimental results, and this punch velocity is proven to be a good compromise between accuracy and effectiveness.

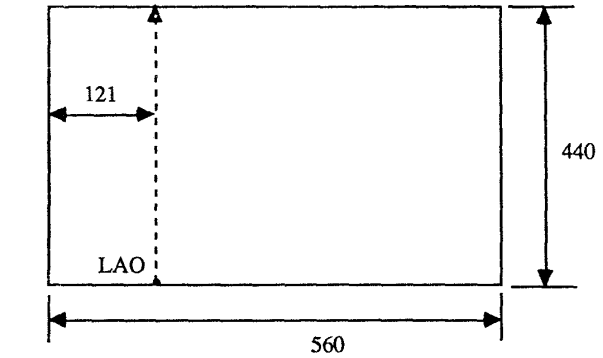

(a)

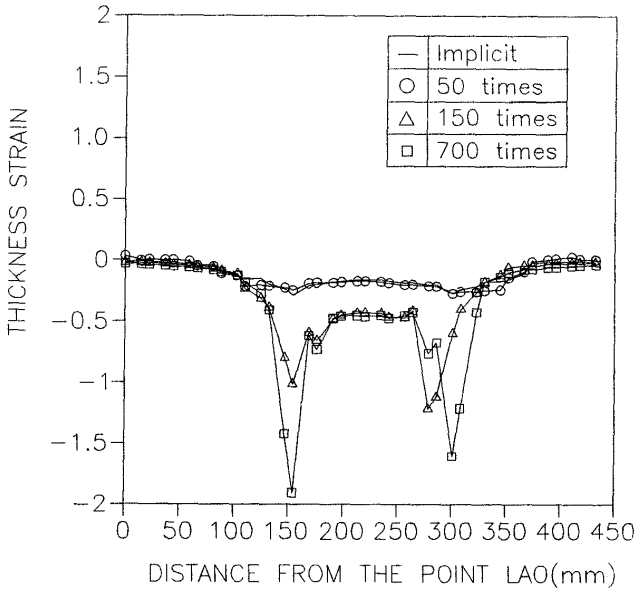

(b)

Fig. 10 Thickness strain distribution for the deep drawing of an oilpan with various mass scaling. (a) Base line on initial sheet blank for strain distribution measurement. (b) Comparison of thickness strain distribution on the line

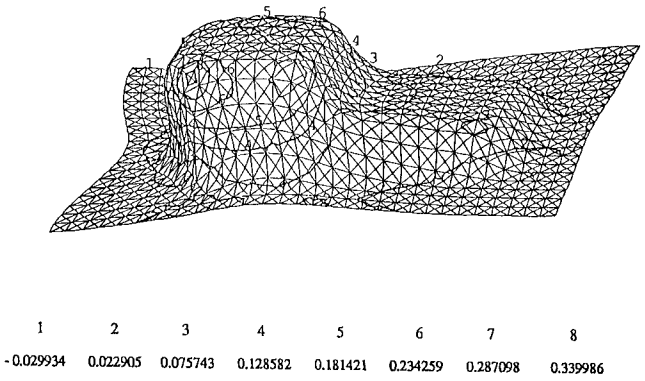

Fig. 11 Thickness strain distribution and deformed configuration of an oilpan predicted by the simulation of the 15 m/s punch velocity and the 50 times mass scaling at the final stage

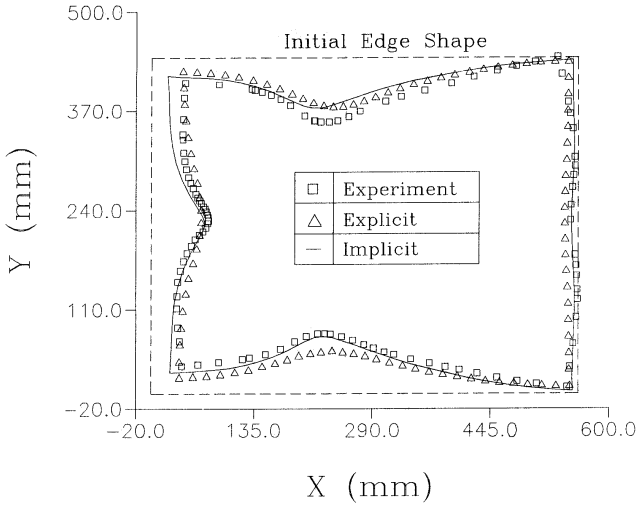

Fig. 12 Comparison of the simulated results of the 15 m/s punch velocity and the 50 times mass scaling with the experiment for the deformed edge shape: deep drawing of an oilpan

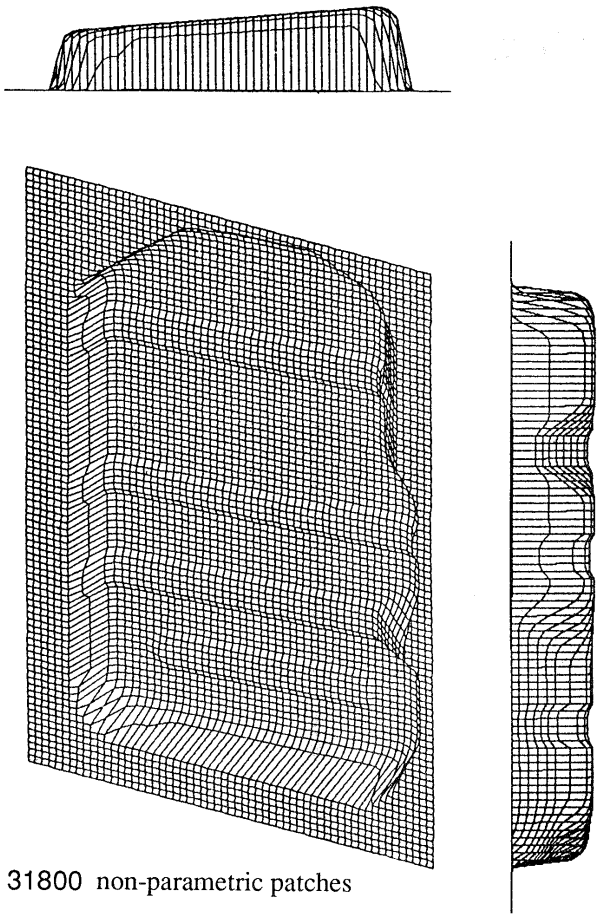

Fig. 13 Schematic view of the nonparametric tool surfaces for fuel tank deep drawing

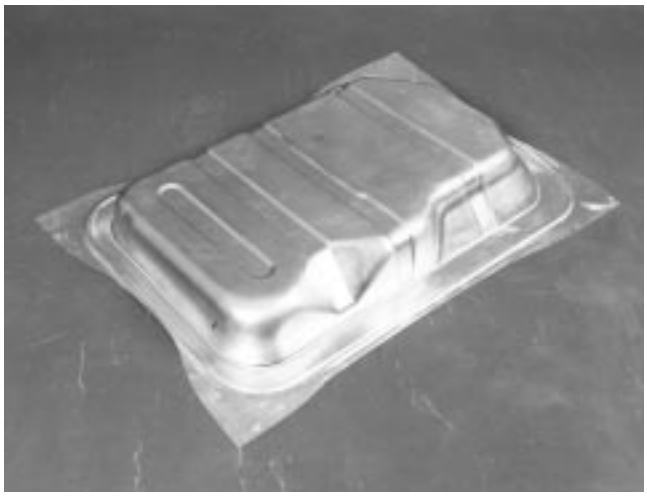

(a)

(b)

Fig. 14 Photographs of experimental specimens by a fuel tank deep drawing. (a) View-1. (b) View-2

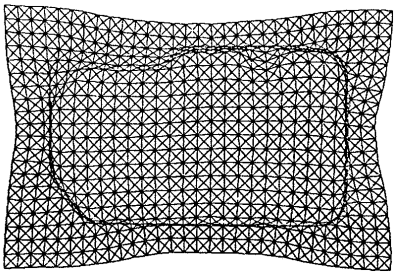

(a)

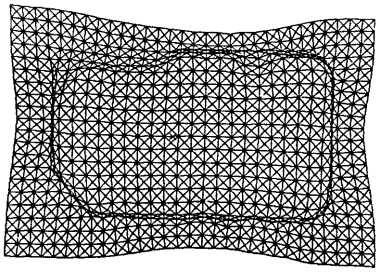

(b)

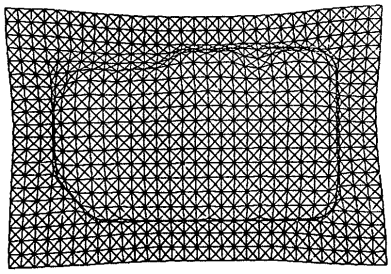

(c)

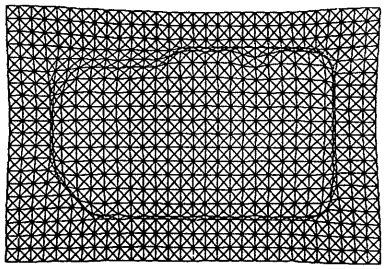

(d)

Fig. 15 Comparison of edge contour in fuel tank deep drawing with various punch velocity. Punch velocity equals (a) 5 m/s, (b) 10 m/s, (c) 20 m/s, and (d) 30 m/s.

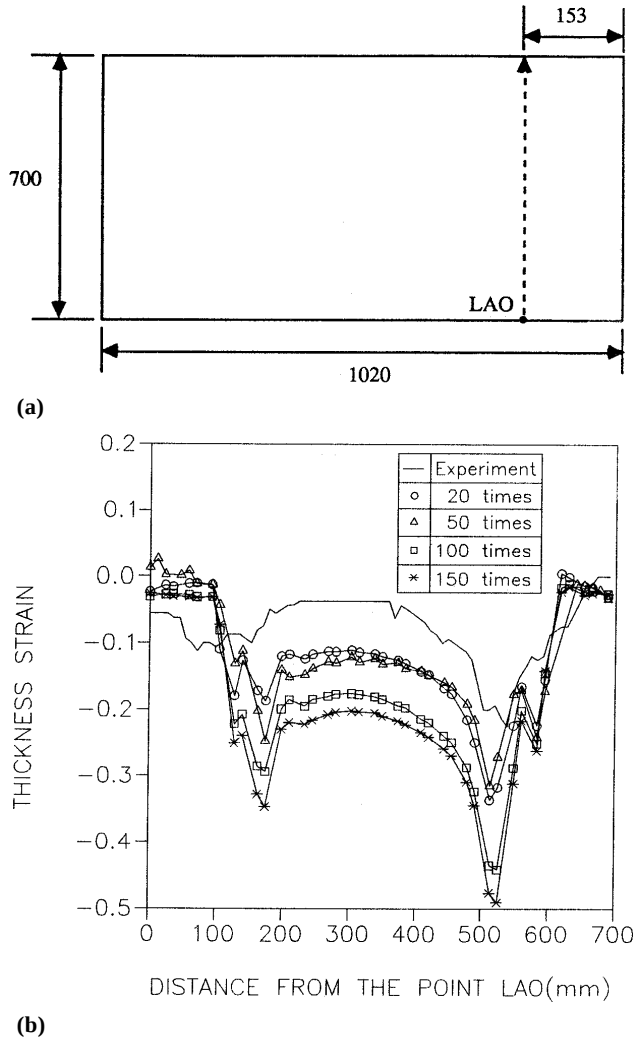

Fig. 16 Thickness strain distribution for the deep drawing of a fuel tank with various punch velocity. (a) Base line on initial sheet blank for strain distribution measurement. (b) Comparison of thickness strain distribution on the line

The whole computation time for the dynamic explicit case of 10 m/s punch velocity took approximately 1 h in Hp/730 workstation. For the dynamic explicit case of 5 m/s punch velocity, it took approximately 1.88 h. For the case of 20 m/s, it took approximately 0.49 h. For the case of 30 m/s, it took approximately 0.18 h.

The mass scaling method is introduced for economic analysis. To investigate the effects of mass scaling, the various mass scalings, which increase the density by factors of 20, 50, 100, and 150, are used with 10 m/s punch velocity. Figure 17 shows the predicted deformed configurations, and Fig. 18 shows the thickness strain distribution at an arbitrarily chosen section. In the case of punch velocity, the excessive increase in the mass scaling causes the deviation from reasonable solution.

This phenomenon can be explained by the excessive increase of inertia energy due to large density. The results of the mass scaling in which the density is increased by a factor of 50 are similar to the results of the mass scaling in which the density is increased by a factor of 20, and these results also agree with

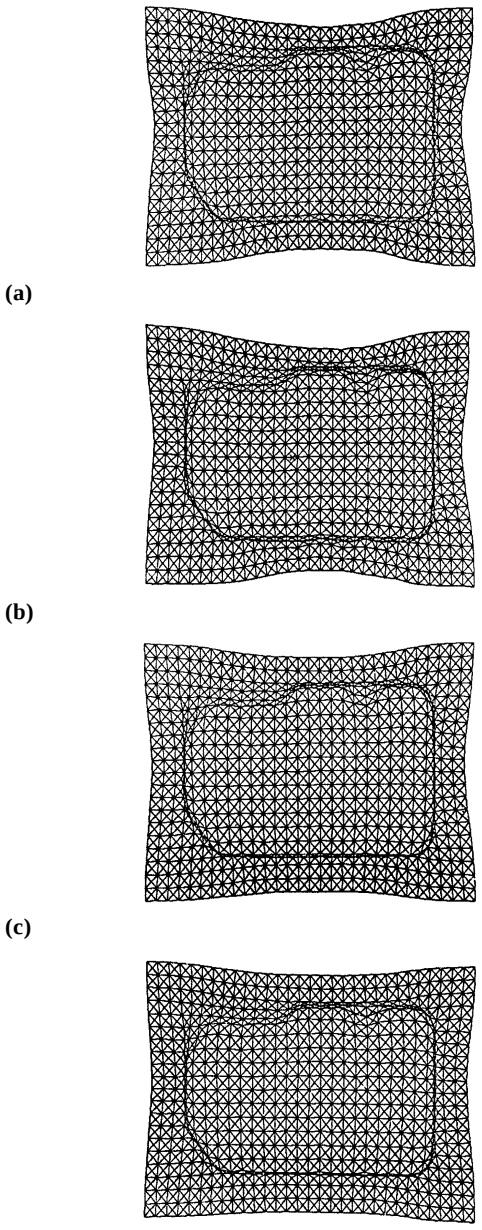

Fig. 17 Comparison of edge contour in fuel tank deep drawing with various mass scaling. Increasing the density by a factor of (a) 20, (b) 50, (c) 100, and (d) 150.

the experimental results. The mass scaling in which the density is increased by a factor of 50 is shown to provide a comparatively reasonable solution. The whole computation time for the dynamic explicit case of the mass scaling, in which the density is increased by a factor of 50, took approximately 1 h in Hp/730 workstation. For the dynamic explicit case of the mass scaling, in which the density is increased by a factor of 20, it took approximately 1.53 h. For the dynamic explicit case of the mass scaling in which the density is increased by a factor of 100, it took approximately 0.69 h. For the dynamic explicit case of the mass scaling, in which the density is increased by a factor of 150, it took approximately 0.58 h. Figure 19 shows the

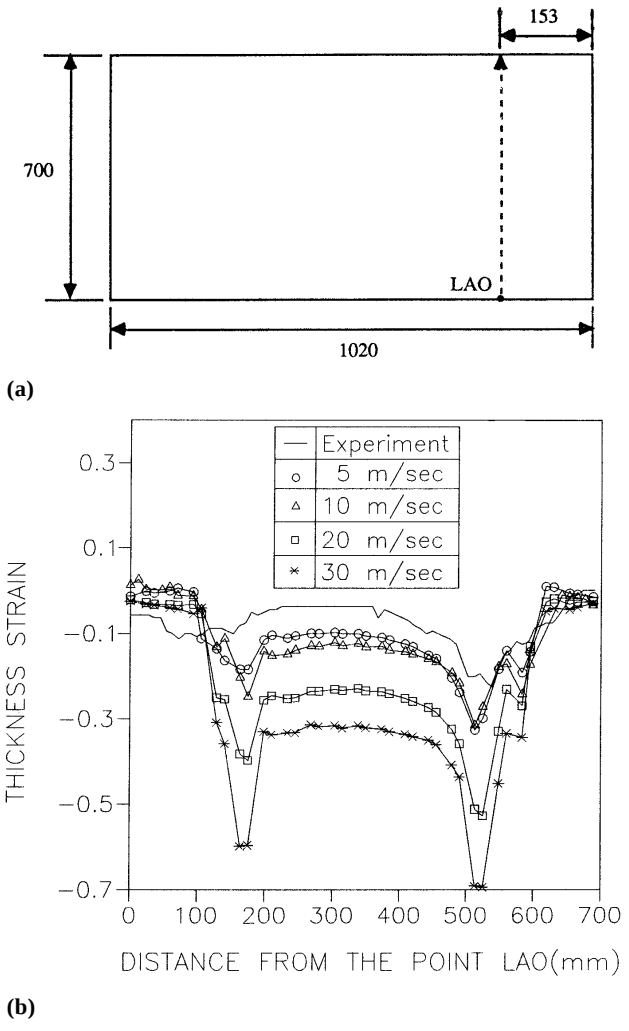

Fig. 18 Thickness strain distribution for the deep drawing of a fuel tank with various mass scaling.(a) Base line on initial sheet blank for strain distribution measurement. (b) Comparison of thickness strain distribution on the line

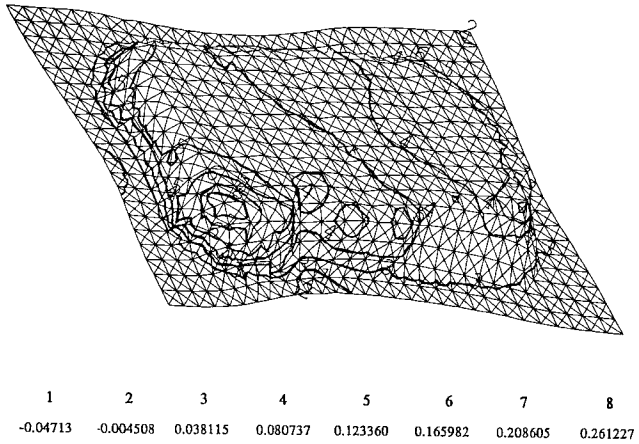

Fig. 19 Thickness strain distribution and deformed configuration of a fuel tank predicted by the simulation of the 10 m/s punch velocity and the 50 times mass scaling at the final stage

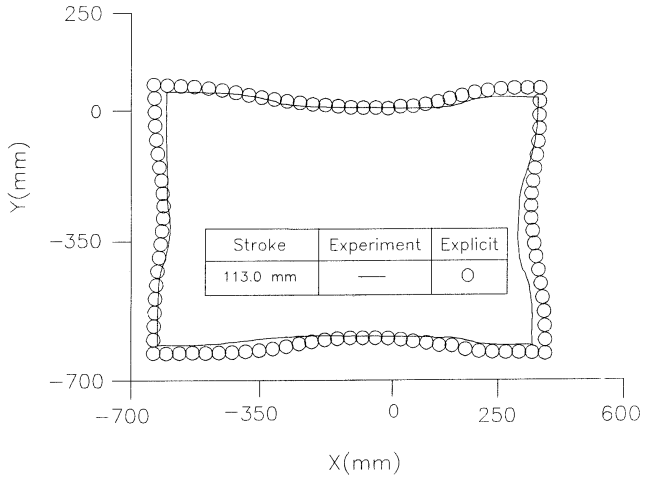

Fig. 20 Comparison of the simulated results of the 10 m/s punch velocity and the 50 times mass scaling with the experiment for the deformed edge shape: deep drawing of a fuel tank

thickness strain distribution and deformed configuration predicted by the simulation of the 10 m/s punch velocity and the 50 times mass scaling at the final stage. Figure 20 shows the comparison of the deformed edge contour predicted by the present analysis of 10 m/s punch velocity and the 50 times mass scaling with the experimental results. The edge contour is somewhat different from the experimental result. This discrepancy is partly due to the ignorance of draw beads. The deviation can be considered from the introduction of many assumptions for the efficient and simple analysis, the limitation of analysis code itself and the measurement error of experimental results, and so on.

4. Conclusions

The dynamic explicit finite element method has been developed and applied to the analysis of sheet metal forming processes. For analyses of more complex cases with larger and more refined meshes, the explicit method is more effective than the implicit method, while the implicit method is widely used because of its excellent accuracy and reliability.

In the explicit analysis, the punch velocity is increased to save computing time at the cost of solution accuracy. As the punch velocity is increased, the inertia effect becomes larger, and force cannot be sufficiently transmitted to the nodes located at the outside of the blank. Also, the deformed configurations of the flange show less drawing-in. Therefore, a reasonable punch velocity should be chosen so that computation time and solution reliability can be compromised so that the inertial effect can be properly controlled.

For economic analysis, the mass scaling method is introduced in the dynamic explicit analysis. As in the case of punch velocity, the excessive increase in the mass scaling causes the deviation from reasonable solution. This phenomenon can be explained by the excessive increase of inertia energy due to

large density. The mass scaling factor, which does not affect solution reliability and is able to provide economic analysis, should be chosen. Also, the inertial effect should be properly controlled. The dynamic explicit analysis is applied to the complicated sheet metal forming processes such as forming of an oilpan and a fuel tank. Additionally, the investigation on the effects of the punch velocity and the mass scaling scheme in the simulation results is conducted.

References

1. N.M. Wang and B. Budiansky, Analysis of Sheet Metal Stamping by a Finite Element Method, *J. Appl. Mech.*, Vol 45, March 1978, p 73-82
2. S.W. Key, R.D. Krieg, and K.J. Bathe, On the Application of the Finite Element Method to Metal Forming Processes, *Comp. Meth. in Appl. Mech. and Eng.*, Vol 17/18, 1979, p 597-608
3. *Proc. of the Second Int. Conf. on Numerical Methods in Industrial Forming Processes,* K. Mattiasson et al., Ed., (Gothenburg, Sweden), 1986
4. *Proc. of the Third Int. Conf. on Numerical Methods in Industrial Forming Processes,* E.G. Thompson et al., Ed., (Fort Collins, Colorado), 1989
5. *Proc. of the Second Int. Conf. on the Technology of Plasticity,* K. Lange et al., Ed., Springer Verlag, Berlin, 1987
6. Modeling of Metal Forming Processes, *Proc. of Euromech Colliquium 233,* J.L. Chenot and E. Onate, Ed., Kluwer, Dordrecht, The Netherlands, Academic Publishers, 1988
7. D.Y. Yang, D.W. Jung, I.S. Song, D.J. Yoo, and J.H. Lee, Comparative Investigation into Implicit, Explicit and Iterative Implicit/Explicit Schemes for the Simulation of Sheet-Metal Forming Processes, *J. Mater. Process. Technol.*, Vol 50, 1995, p 39-53
8. R.D. Wood, J. Bont, and A.H.S. Wargadipurea, Simulation of the Superplastic Forming of Thin Sheet Components using the Finite Element Method, *Proc. Third Int. Conf. on Num. Meth. in Ind. Forming Proc.,* E.G. Thompson et al., Ed., (Fort Collins, Colorado), 1989
9. N. Rebelo, J.C. Nagtegaal, and H.D. Hibbitt, Practical Aspects of Modeling Sheet Forming Processes, *Proc. Third Int. Conf. on Num. Meth. in Ind. Forming Proc.,* E.G. Thompson et al., Ed., (Fort Collins, Colorado), 1989
10. J.B. Dalin and E. Onate, An Automatic Algorithm for Contact Problems: Application to Sheet Metal Forming, *Proc. Third Int. Conf. on Num. Meth. in Ind. Forming Proc.,* E.G. Thompson et al., Ed., (Fort Collins, Colorado), 1989
11. D.W. Jung, D.J. Yoo, and D.Y. Yang, A Dynamic Explicit/Rigid-Plastic Finite Element Formulation and Its Application to Sheet Metal Forming Processes, *Eng. Computations,* Vol 12, 1995, p 707-722
12. *Proc. of the Fifth Int. Conf. on the Technology of Plasticity,* T. Altan et al., Ed., (Columbus, Ohio), 1996
13. *Abaqus/Explicit: User's Examples and Theory Manuals,* Hibbitt, Karlsson & Sorensen, Inc., 1991
14. J.C. Nagtegaal and L.M. Taylor, Comparison of Implicit and Explicit Finite Element Methods for Analysis of the FE-Sim. of 3-D Sheet Metal Forming Processes, in *Automotive Ind. Conf.,* J. Reissner et al., Ed., VDI Verlag, Dusseldorf, 1991
15. E. Hinton, T. Rock, and O.C. Zienkiewicz, A Note on Mass Lumping and Related Processes in the Finite Element Method, *Earthquake Eng. Struct. Dynamics,* Vol 4 (No. 3), 1976, p 145-149
16. K.S. Surana, Lumped Mass Matrices with Non-Zero Inertia for General Shell and Axisymmetric Shell Elements, *Int. J. Numer. Methods Eng.,* Vol 12 (No. 11), 1978, p 1635-1650
17. P.T. Vreede, M.F.M. Louwes, and J. Huetink, Contact Behaviour Modelled with Interface Elements and Tool Description, *Proc. NUMIFORM '92 Conf.,* A.A. Rotterdam, Ed., (Brookfield), Balkema Publishers, 1992, p 565-570
18. S.D. Liu and M. Karin, A One Step Finite Element Approach for Product Design of Sheet Metal, *Proc. NUMIFORM '92 Conf.,* A.A. Rotterdam, Ed., (Brookfield), Balkema Publishers, 1992, p 497-502
19. T. Huo and E. Nakamachi, Evaluation of Dynamic Explicit/Elasto Viscoplastic Finite Element Method in Sheet Forming Simulation, *NUMISHEET '93, Second Int. Conf. of Numerical Simulation of 3-D Sheet Metal Forming Processes—Verification of Simulations with Experiments,* (Tokyo, Japan), 1993, p 173-186
20. W.J. Chung, J.W. Cho, and T. Belytschko, A Study on Dynamic Effects of Dynamic Explicit FEM in Sheet Metal Forming Analysis, *NUMISHEET '96, Third Int. Conf. of Numerical Simulation of 3-D Sheet Metal Forming Processes—Verification of Simulations with Experiments,* (Dearborn, Michigan), 1996, p 414-420
21. D.J. Yoo, " Analysis of Three-Dimensional Sheet Metal Forming Processes Using Continuous Surface and Contact Treatment," Ph.D. thesis, Korea Advanced Institute of Science and Technology, 1994